

Geometrical optimization of high speed intra-cavity-contacted oxide-confined VCSELs

V. V. LYSAK^{a,b}, YONG TAK LEE^a

^aDepartment of information and communication, Gwangju Institute of science and technology (GIST), 1 Oryong-dong, Buk-ku, Gwangju, 500-712, Republic of Korea

^bLaboratory "Photonics", Kharkov National University of Radio Electronics, 14, Lenin av., Kharkov, 61166, Ukraine

In this work, the simulation of the 980 nm InGaAs intra-cavity-contacted oxide-confined vertical-cavity surface-emitting lasers is presented including the thermal effects. We analyze the thermal, electrical and optical properties of such devices with the different thicknesses of contact layers. Results of simulations show the larger optical power for devices with thicker contact layers. The device with contact layers of $5\lambda/4n$ thickness has the maximal modulation bandwidth.

(Received June 28, 2006; accepted July 20, 2006)

Keywords: DC characteristics, Intracavity-contacted oxide-confined vertical-cavity surface-emitting laser, Modulation bandwidth

1. Introduction

Vertical-cavity surface-emitting lasers (VCSEL's) have bandwidths greater than 10 GHz and they are expected to play a key role for next-generation network transceivers [1]. Over short distances inside computer systems or clusters of electronic networks, board-to-board or chip-to-chip multi gigahertz bandwidth optical interconnects are required to replace electrical interconnects. The optical interconnects include direct interconnects among boards, arbitrary interconnection patterns, channel isolation, and increased bandwidth, thus, avoiding the interconnection bandwidth bottleneck of systems with strictly in-plane electronic interconnects. Optical interconnects can be used in an increasing number of applications related to high data rate real time operations such as short distance networks, signal processing boards, etc. [2].

VCSELs can be divided into two contacting schemes: extracavity - (EC) and intracavity - contacted (IC) structures. In the extracavity case, the carrier is injected into the active region by passing through the Distributed Bragg Reflector (DBR) mirror stack. In order to reduce the driving voltage and improve their power conversion efficiency the DBR resistance is decreased by grading the interfaces and making complex doping profiles that increase the optical losses [3]. In the intracavity-contacted oxide-confined VCSELs (ICOC-VCSELs) the active region is bordered by two highly doped contact layers to inject current. In this case, the current bypasses the substrate and both DBRs and hence the undoped mirrors without graded interfaces or dielectric mirrors, which minimize the optical losses, can be made [4].

In conventional EC VCSELs, the current travels about 3 μm vertically, and through the many heterointerfaces. This allows effective current spreading. However, in the ICOC VCSELs, the current flows in the horizontal direction because of the thinner contact layer, and there is not enough room for uniform carrier redistribution into the active layer as it travels through the spacer layers. Thus, it

leads to a heavy current crowding at the rim of the oxide window resulting in higher optical losses and lower modulation bandwidth [1]. To suppress the current crowding effect, the thickness of graded layer (GLT) at contact layer-oxide window aperture interface is optimized [5].

In this paper, we show that an optimal thickness of contact layer can suppress the current crowding more effectively and improve the modulation characteristics.

2. Structure description

The schematic representation of the simulated 980 nm ICOC VCSEL is presented in Figure 1. The active layer contains three 70 \AA $\text{In}_{0.2}\text{Ga}_{0.8}\text{As}$ quantum wells (QWs), separated by 150 \AA GaAs barrier between the 200 \AA separate confinement heterostructure (SCH) barriers. The resonator contains two $\text{Al}_{0.3}\text{Ga}_{0.7}\text{As}$ cladding layers. Oxide windows next to the quantum-well active region are formed by the lateral selective steam oxidation of AlAs to guide the current (to funnel current spreading from annular contact into the central active region), as well as the optical mode (to confine an optical field in radial direction) through the central region of the resonator [6]. The 60 \AA graded layer is placed at the contact layer-oxide window aperture interface for both p- and n-contacts [5]. The width of the p- and n-contacts is 10 μm . The diameter of oxide window aperture is 14 μm and the diameter of top DBR mirror is 20 μm . The top and bottom Bragg reflector stacks consist of 25 $\text{Al}_{0.9}\text{Ga}_{0.1}\text{As}/\text{GaAs}$ and 27 AlAs/GaAs layer pairs, respectively. While p- and n-contact layers are parts of DBR mirrors, the thickness of ones will be changed by law: $d=(2k+1)\lambda/4n$, where d is the contact layer thickness, $k=0, 1, 2, \dots$, λ is the operation wavelength, n is the refractive index of layer.

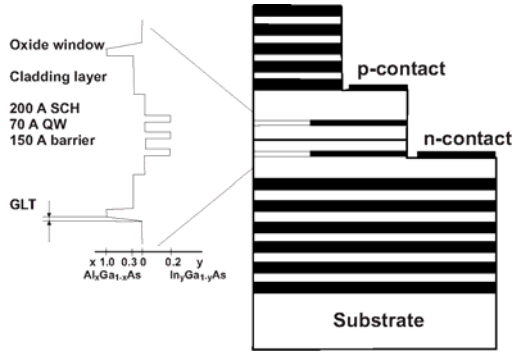


Fig. 1. Intracavity-contacted oxide-confined (ICOC) VCSEL structure.

3. Numerical simulations and description of results

In this work, the self-consistent modeling software PICS3D is used for simulating of the structure [7]. This software simulates a wide spectrum of electrical, optical and thermal characteristics with the ability to update to new material parameters and calculation algorithms. All important heat sources, i.e. non-radiative recombination, absorption of spontaneous radiation, as well as volume and Joule heating are taken into account. The main material parameters can be found in the related literature [8, 9].

Fig. 2 shows the voltage-current (V-I) (Fig. 2a) and light-current (L-I) (Fig. 2b) characteristics for different values of the contact layer thickness (CLT) (1, 3, 5 and 7 quarter-wave thickness, respectively), which are same for both n- and p-contact sides.

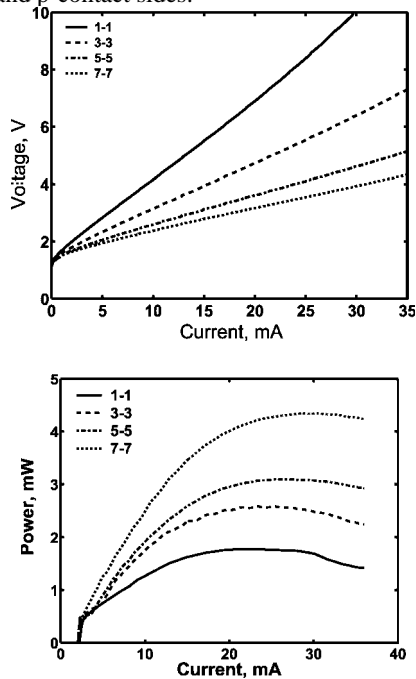


Fig. 2. a) V-I and b) L-I characteristics for different values of n- and p- contact layer thickness of $\lambda/4n$ (solid lines), $3\lambda/4n$ (dashed lines), $5\lambda/4n$ (dash-dotted lines) and $7\lambda/4n$ (dotted lines).

V-I characteristics clarify that increasing the CLT decreases the differential resistance due to decrease of the contact layer resistance that confirms the previous analytical investigations of contact layer resistance [10]. The nature of L-I characteristics show the larger slope efficiency and maximal output power for device with thicker contact layers. In Fig. 3, we present the radial distribution of lattice temperature in the central quantum well at pumping current of 10 mA. Fig. 2 and Fig. 3 clarify that the device with lower resistance has smaller temperature in the active layer and less temperature gain suppression.

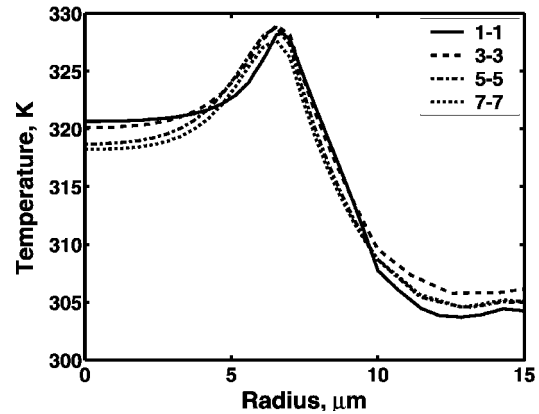


Fig. 3. Radial distribution of the lattice temperature in active layer with different values of CLT.

Fig. 4 shows the radial distribution of the hole concentration in the active layer of the ICOC VCSEL with different values of CLT at pumping current of 10 mA. As the CLT is reduced, the carrier distribution in the active layer becomes more uniform because thinner contact layer with larger resistance suppresses the current crowding. That results in a more uniform carrier distribution in the active layer [5]. The current crowding does not effect on the slope efficiency, but has some influence on the modulation properties as we will show below.

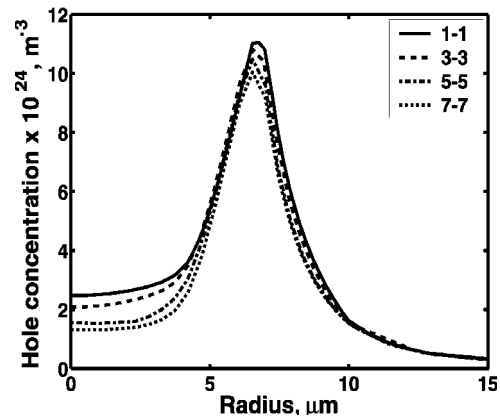


Fig. 4. Radial distribution of the electron concentration in active layer with different values of CLT.

The modulation properties of VCSEL can be predicted by the relaxation resonance. For bias currents

sufficiently far above threshold to ensure effective carrier clamping, the frequency of this resonance is given by [11]:

$$f_R = \frac{1}{2\pi} \sqrt{\eta_i \frac{\Gamma \xi v_g}{q V_{eff}} \frac{\partial g}{\partial N} (I - I_{th})},$$

where η_i is the internal quantum efficiency; Γ is the confinement factor; ξ is the energy confinement factor or gain enhancement factor; q is the electron charge; V_{eff} is the effective volume of resonator including the penetration depth of DBR mirrors; $\partial g/\partial N$ is the differential gain; I is the bias current, and I_{th} is the threshold current. Additionally, the resonant frequency is limited by the RC parasitic via: $f_R \sim (R_{tot} C_{par})^{-0.5}$, where R_{tot} is the total device resistance and C_{par} is the parasitic capacitance.

Fig. 5 shows the 3-dB frequency dependence of the device on $\sqrt{I - I_{th}}$ for different CLT values. Calculated data for devices with 1, 3, 5 and 7 quarter-wave CLT are presented by squares, triangles, circles and diamonds, respectively and the modulation conversion efficiency factor is approximately 3.49, 5.06, 5.92 and 5.56 GHz/(mA)^{0.5}, respectively.

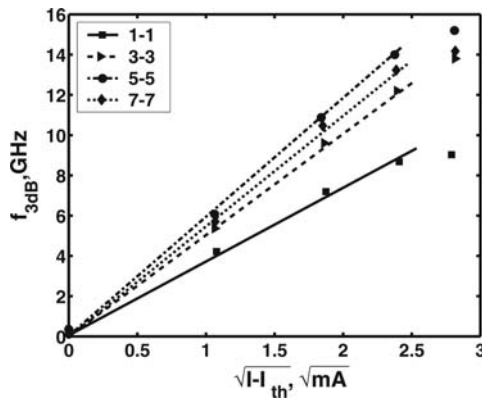


Fig. 5. The modulation conversion efficiency factor of ICOC VCSELs with different values of CLT.

Decreasing the CLT increases the differential resistance (see V-I characteristics in Fig. 2). On the other hand, increasing the CLT changes the parameters as follows:

- increases the effective volume of resonator and decreases the gain enhancement factor due to increasing the penetration depths of DBR mirrors [11];
- reduces differential gain from the current crowding effect (see Fig. 4).

Both processes decrease the resonant frequency when pushed too far and there is some optimal CLT range for which the modulation bandwidth is the widest. Results of simulation show that the devices with CLT of about $5\lambda/4n$

have maximum bandwidth over a wide region of pumping currents.

4. Conclusion

In summary, we have analyzed the thermal, electrical, optical, and modulation properties of the 980 nm InGaAs ICOC VCSELs with different values of p- and n-contact layer thickness. Results show that increasing CLT increases the slope efficiency of L-I characteristic and decreases the resistance of device. The analysis of modulation characteristics clarify that devices with the optimal CLT of $5\lambda/4n$ have the widest modulation bandwidth and the modulation conversion efficiency factor is approximately 5.92 GHz/(mA)^{0.5} due to compromise between the effective volume of resonator, current crowding suppression and total resistance.

Acknowledgement

This work is supported by MOE through the BK21 Program and by MOST through TND Project of Korea.

References

- [1] A. V. Krishnamoorthy, L. M. F. Chirovsky, W. S. Hobson, J. Lopata, J. Shah, R. Rozier, J. E. Cunningham, and L. A. D'Asaro, IEEE Photon. Technol. Lett. **12**, 609 (2000).
- [2] K.-M. Chu, J.-S. Lee, H.-S. Cho, H.-H. Park, D.-Y. Jeon, IEEE Trans. on Electronics packaging manufacturing **27**, 246 (2004).
- [3] K. L. Lear, S. A. Chalmers, IEEE Photon. Technol. Lett., **5**, 972 (1993).
- [4] J. W. Scott, B. J. Thibeault, D. B. Young, L. A. Coldren, F. H. Peters, IEEE Photon. Technol. Lett. **6**, 678 (1994).
- [5] V. V. Lysak, K. S. Chang, Y. T. Lee, Appl. Phys. Lett. **87**, 231118 (2005).
- [6] R. P. Sarzala, IEEE J. Quantum Electron. **40**, 629 (2004).
- [7] PICS3D, User's manual and reference manual, version 2002.2, Crosslight Inc., 2002.
- [8] S. M. SZE, Physics of semiconductor devices, 2nd edition (Wiley, New York, 1981), Chap. 1-7, p.279.
- [9] J. Piprek, Semiconductor optoelectronics devices. Introduction to physics and simulation (Academic Press, Amsterdam, 2003), p.279.
- [10] M. H. MacDougal, J. Geske, C.-K. Lin, A. E. Bond, P. D. Dapkus, IEEE Photon. Technol. Lett. **10**, 9 (1998).
- [11] Vertical cavity surface emitting lasers: design, fabrication, characterization, and application/ Eds. Carl Wilmsen, Henryk Temkin, Larry A. Coldren, 455 p., Cambridge University Press, 1999

*Corresponding author: ytle@gist.ac.kr